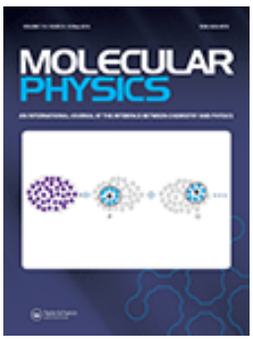

Taylor & Francis
Taylor & Francis Group

Molecular Physics

An International Journal at the Interface Between Chemistry and Physics

ISSN: (Print) (Online) Journal homepage: https://www.tandfonline.com/loi/tmph20

Excited states of molecular and crystalline acetylene: application of TDHF and BSE via density fitting methods

C. H. Patterson

To cite this article: C. H. Patterson (2020): Excited states of molecular and crystalline acetylene: application of TDHF and BSE via density fitting methods, Molecular Physics, DOI: 10.1080/00268976.2020.1792568

To link to this article: https://doi.org/10.1080/00268976.2020.1792568

Published online: 13 Jul 2020.

MOLECULAR PHYSICS
https://doi.org/10.1080/00268976.2020.1792568

Taylor & Francis
Taylor & Francis Group

60TH SANIBEL SYMPOSIUM

Excited states of molecular and crystalline acetylene: application of TDHF and BSE via density fitting methods

C. H. Patterson

School of Physics, Trinity College Dublin, Dublin, Ireland

ABSTRACT

Low-lying states in small, multiply bonded hydrocarbon molecules may be divided into valence and Rydberg excitations. Excited states of the cubic phase of the acetylene molecular crystal are calculated using the time-dependent Hartree–Fock (TDHF) method. TDHF and Bethe–Salpeter equation (BSE) calculations are performed on molecular C_2H_2 in order to interpret these excited states. Computationally inexpensive TDHF and BSE methods are compared to previous CASPT2, MRCI and EOM-CCSD calculations and experiment. Localised, lowest energy excited states in the C_2H_2 molecular crystal mirror those in the gas phase. In the next lowest excitations the electron and hole separate over one or two shells of molecular neighbours. A density fitting method for calculating the Coulomb matrix elements which arise in time-dependent Hartree Fock theory (TDHF) in periodic systems is implemented in the Exciton code and described briefly.

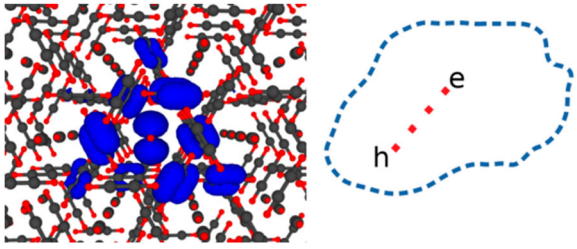

ARTICLE HISTORY
Received 6 May 2020
Accepted 1 July 2020

KEYWORDS
Time-dependent Hartree–Fock; Bethe–Salpeter equation; molecular crystal; acetylene; excitons

1. Introduction

Condensed organic phases have applications as light emitters and absorbers as organic light-emitting diodes and as photovoltaic materials and many questions remain regarding their excited states and charge transfer processes [1,2]. Excited states of small organic molecules such as C_2H_2 have been studied extensively in the gas phase, both by experiment [3–6] and high-level quantum chemistry methods [7–10]. Interest stems partly from the importance of C_2H_2 in astrophysics [5,6]. Here we report time-dependent Hartree–Fock (TDHF) and *GW*/Bethe–Salpeter equation (BSE) calculations [11–13] on molecular C_2H_2 and TDHF calculations in the Tamm-Dancoff approximation (TDA) on the cubic phase of the C_2H_2 molecular crystal [14]. This herringbone phase has 4 formula units per cell, space group $Pa\bar{3}$ (No. 205) and an experimental lattice constant of 6.105 Å. Extensive benchmarking has been done for the BSE method applied to small organic molecules [15–17].

Excitations of C_2H_2 below the ionisation threshold of 11.40 eV [18] consist of valence and Rydberg states. Valence excitations of C_2H_2 have cis- or trans-bent minimum energy configurations [19] which lie 1 or 2 eV below the vertical excitation energies from the ground state. Rydberg states in molecules require extensive diffuse functions in a local orbital basis set. Here we compare inexpensive TDHF and BSE calculations which used TZVPPD basis sets [20–22] with limited diffuse functions to more accurate but computationally expensive CASPT2 [7], CMRCI+Q [9] and EOM-CCSD [10] calculations which used extensive valence and diffuse basis sets.

Results of these calculations are also compared to TDHF-TDA calculations on the C_2H_2 molecular crystal.

CONTACT C. H. Patterson charles.patterson@tcd.ie School of Physics, Trinity College Dublin, Dublin 2, Dublin, Ireland

Inclusion of diffuse Gaussian type orbitals (GTO) in Hartree–Fock (HF) calculations on systems with periodic boundary conditions is limited by potential linear dependence of the basis set and divergence of the exchange part of the SCF Hamiltonian. The former arises from strong overlap of diffuse functions on neighbouring atoms and the latter from the $\mathbf{q} \to 0$ singularity of the HF exchange potential in periodic systems. A modified TZVPPD basis for C and H was used in these calculations. Omission of diffuse GTO with exponents less than 0.1 a_o^{-2} is ameliorated by basis sets on adjacent atoms. In order to ascertain the effect of omission of diffuse functions on the excitation spectrum of molecular C_2H_2, calculations were performed using the TZVPPD basis and the modified TZVPPD basis for both a single molecule in free space and a molecule in a large box with periodic boundary conditions.

All calculations in this work were done using the Exciton code [23,24]. The *GW* and BSE/TDHF calculations reported below each require less than 4 CPU seconds on a single core for an active space containing 3 valence states and 44 virtual states in the full TZVPPD basis, including integral generation and Hamiltonian diagonalisation. Integrals in the *GW* self-energy and *A* and *B* matrices in TDHF and BSE calculations are generated using a density fitting method, which is described below.

1.1. Overview of experimental and theoretical results

The original observation of the VUV absorption spectrum of C_2H_2 was made by Price in 1935 [25]. A high resolution (e, e) dipole spectroscopy study by Cooper *et al.* [3] includes a summary of experimental work to 1995 and reports oscillator strengths for the $\tilde{A} \leftarrow \tilde{X}, \tilde{B} \leftarrow \tilde{X}$ and $\tilde{E} \leftarrow \tilde{X}$ bands as well as four Rydberg excitations denoted *R* to *R*‴. Oscillator strengths for these transitions have been revisited more recently via synchrotron VUV absorption [5] and high energy electron scattering [6].

Potential energy surfaces of valence excitations of C_2H_2 have been investigated using CI methods by Perić and coworkers [26–28]. Malsch and coworkers [7] reported CASSCF and CASPT2 calculations of vertical excitations of singlet and triplet Rydberg states in C_2H_2 as well as geometries of singlet and triplet valence excited states. Outer-valence Green functions (OVGF) and equation-of-motion coupled cluster (EOM-CCSD) with specially constructed basis sets have been carried out to predict Rydberg excitation energies of acetylene with principal quantum numbers up to $n = 11$ by Zyubin and Mebel [8]. Laruelle and coworkers [9] reported contracted multireference CI with quadruples corrections (CMRCI+Q) on C_2H_2, including over 20 different excited states. Recent EOM-CCSD calculations by Watanabe and Takahashi [10] find good agreement with these last two works for nine valence and Rydberg excitations.

Excitations are divided into 'valence' and 'Rydberg' excitations in which the excited state is either cis- or trans-bent or linear. The C_2H_2 molecular ion is linear and hence Rydberg excitations can also be expected to have linear molecular configurations. Malsch and coworkers [7] and Laruelle and coworkers [9] calculated potential energy curves for the valence excitations and found adiabatic excitation energies for the cis-bent S_1 state of 5.55 eV (CASPT2) and 5.14 eV (CASPT2) for the trans-bent state. Here we consider only vertical excitations from the HF equilibrium geometry and the experimental geometry of the C_2H_2 molecular crystal.

2. Theoretical background

2.1. TDHF and GW/BSE approach

The TDHF and BSE equations are usually expressed as the following generalised eigenvalue problem,

$$\begin{pmatrix} A & B \\ -B^* & -A^* \end{pmatrix} \begin{pmatrix} X \\ Y \end{pmatrix} = \Omega \begin{pmatrix} X \\ Y \end{pmatrix}. \qquad (1)$$

Matrix elements for both TDHF and BSE for molecules with occupied orbitals, *i*, *j*, and virtual orbitals, *a*, *b*, are summarised in Table 1, where both *A* and *B* blocks of the matrix are given in chemists notation so that,

$$(ai|jb) = \left(\phi_a^*(\mathbf{r})\phi_i(\mathbf{r})|\phi_j^*(\mathbf{r}')\phi_b(\mathbf{r}')\right). \qquad (2)$$

Note that the TDA amounts to setting the *B* blocks to zero. *A* and *B* blocks in TDHF and BSE differ in that two terms in BSE employ a screened Coulomb potential, $W_0(0)$, while all matrix elements in TDHF employ the unscreened Coulomb potential. The former is indicated by $|W_0(0)|$ and the latter by | in Table 1. In TDHF for periodic systems with occupied states, $v\mathbf{k}, v'\mathbf{k}+\mathbf{q}$, and conduction states, $c\mathbf{k}, c'\mathbf{k}+\mathbf{q}$, at wave vectors $\mathbf{k}$ and $\mathbf{k}+\mathbf{q}$, the $A_{cv\mathbf{k},c'v'\mathbf{k}+\mathbf{q}}$ matrix elements are replaced by electron-hole hopping (ring diagram) matrix elements,

$$2\left(\Psi_{c\mathbf{k}}^*(\mathbf{r})\Psi_{v\mathbf{k}}(\mathbf{r})|\Psi_{v'\mathbf{k}+\mathbf{q}}^*(\mathbf{r}')\Psi_{c'\mathbf{k}+\mathbf{q}}(\mathbf{r}')\right), \qquad (3)$$

and electron-hole attraction (ladder diagram) matrix elements,

$$-\left(\Psi_{c\mathbf{k}}^*(\mathbf{r})\Psi_{c'\mathbf{k}+\mathbf{q}}(\mathbf{r})|\Psi_{v'\mathbf{k}+\mathbf{q}}^*(\mathbf{r}')\Psi_{v\mathbf{k}}(\mathbf{r}')\right). \qquad (4)$$

In a *GW*/BSE calculation the single-particle energy differences are quasi-particle energy differences in which the HF energy differences are shifted by matrix elements

Table 1. Table of matrix elements of A and B blocks of Equation (1) for TDHF and BSE approximations for a spin singlet molecule. Factors of two arise from summation over spin, tildes on energy eigenvalues for BSE indicate G_0W_0@HF eigenvalues and $W_0(0)$ is the static, screened Coulomb interaction.

Method	Matrix block	Matrix elements
TDHF	$A_{ai,bj}$	$(\epsilon_a - \epsilon_i)\delta_{ab}\delta_{ij} + 2\,(\mathrm{ai}\vert\mathrm{jb}) - (\mathrm{ab}\vert\mathrm{ji})$
	$B_{ai,bj}$	$2\,(\mathrm{ai}\vert\mathrm{bj}) - (\mathrm{aj}\vert\mathrm{bi})$
BSE	$A_{ai,bj}$	$(\widetilde{\epsilon}_a - \widetilde{\epsilon}_i)\delta_{ab}\delta_{ij} + 2\,(\mathrm{ai}\vert\mathrm{jb}) - (\mathrm{ab}\vert W(0)\vert\mathrm{ji})$
	$B_{ai,bj}$	$2\,(\mathrm{ai}\vert\mathrm{bj}) - (\mathrm{aj}\vert W(0)\vert\mathrm{bi})$

of the dynamic part of the random phase approximation (RPA) self-energy [24]. In a TDHF calculation the single-particle energy differences are HF energy eigenvalue differences.

2.2. Coulomb matrix elements via density fitting

Density fitting (DF) is a long-established technique in both finite [29–31] and periodic systems [32–38]. We briefly describe a DF method for computing the Coulomb matrix elements over Bloch functions or molecular orbitals in Equations (3) and (4). Computation of these matrix elements consumes a large fraction of the time required in a BSE or TDHF calculation for molecular and, especially, periodic systems. When a local orbital basis set is used for DF in a periodic system, methods capable of treating the long-range nature of the Coulomb interaction between local orbital basis functions are essential. Summing interactions in real space is not viable owing to the long-range character of the Coulomb interaction. Here an Ewald approach is outlined which is described in more detail elsewhere [39].

Wave functions $\Psi_{v\mathbf{k}}(\mathbf{r})$ and $\Psi_{c\mathbf{k}+\mathbf{q}}(\mathbf{r})$ are valence and conduction band states at wave vectors $\mathbf{k}$ and $\mathbf{k}+\mathbf{q}$. Bloch functions are expanded as linear combinations of phase-modulated local orbitals, $\phi_m(\mathbf{r}-\mathbf{R})$, in the unit cell with lattice translation vector, $\mathbf{R}$, as crystal orbitals (CO) with wave vector, $\mathbf{k}$,

$$\Psi_{v\mathbf{k}}(\mathbf{r}) = \sum_{m,\mathbf{R}} d_m^{v\mathbf{k}} \phi_m(\mathbf{r}-\mathbf{R}) e^{i\mathbf{k}.\mathbf{R}}. \tag{5}$$

Expansion of Bloch function products in Equations (3) and (4) leads to products of CO basis functions,

$$\rho_{mn}^{\mathbf{q}}(\mathbf{r}) = \sum_{\mathbf{A},\mathbf{B}} \phi_m^*(\mathbf{r}-\mathbf{A})\phi_n(\mathbf{r}-\mathbf{B}) e^{-i\mathbf{k}.\mathbf{A}+i(\mathbf{k}+\mathbf{q}).\mathbf{B}}. \tag{6}$$

An auxiliary fitting basis of the form,

$$\chi_\alpha^{\mathbf{q}}(\mathbf{r}) = \sum_{\mathbf{R}} \chi_\alpha(\mathbf{r}-\mathbf{R}) e^{i\mathbf{q}.\mathbf{R}}, \tag{7}$$

is used to expand CO basis function products in Equation (6). This is generally a much more extensive Gaussian orbital basis set than the CO basis used to expand Bloch functions in Equation (5). Four centre Coulomb integrals over Bloch functions in Equations (3) and (4) require evaluation of integrals of the form,

$$\int \mathrm{d}\mathbf{r}\,\mathrm{d}\mathbf{r}' \frac{\rho_{mn}^{\mathbf{q}}(\mathbf{r})\rho_{rs}^{\mathbf{q}*}(\mathbf{r}')}{|\mathbf{r}-\mathbf{r}'|}.$$

When a Coulomb metric is used in fitting these integrals the quantity,

$$\left\langle \rho_{mn}^{\mathbf{q}}(\mathbf{r}) - c_\alpha^{\mathbf{q}}\chi_\alpha^{\mathbf{q}}(\mathbf{r}) \middle| \rho_{rs}^{*\mathbf{q}}(\mathbf{r}') - c_\beta^{*\mathbf{q}}\chi_\beta^{*\mathbf{q}}(\mathbf{r}') \right\rangle, \tag{8}$$

is minimised. The coefficients, $c_\alpha^{\mathbf{q}}$, which minimise this error are given by [39],

$$c_\alpha^{\mathbf{q}} V_{\alpha\beta}^{\mathbf{q}} = V_{mn\beta}^{\mathbf{q}}. \tag{9}$$

The quantities $V_{\alpha\beta}^{\mathbf{q}}$ and $V_{mn\beta}^{\mathbf{q}}$ are defined by,

$$V_{\alpha\beta}^{\mathbf{q}} = \sum_{\mathbf{A}} \int \mathrm{d}\mathbf{r}\,\mathrm{d}\mathbf{r}' \frac{\chi_\alpha(\mathbf{r})\chi_\beta^*(\mathbf{r}')}{|\mathbf{r}-\mathbf{r}'-\mathbf{A}|} e^{-i\mathbf{q}.\mathbf{A}} \tag{10}$$

and,

$$V_{mn\beta}^{\mathbf{q}} = \sum_{\mathbf{B},\mathbf{C}} \int \mathrm{d}\mathbf{r}\,\mathrm{d}\mathbf{r}' \times \frac{\phi_m^*(\mathbf{r})\phi_n(\mathbf{r}-\mathbf{C})\chi_\beta^*(\mathbf{r}')}{|\mathbf{r}-\mathbf{r}'-\mathbf{B}|} e^{i(\mathbf{k}+\mathbf{q}).\mathbf{C}} e^{-i\mathbf{q}.\mathbf{B}}. \tag{11}$$

Substitution of the expansion of the density, $\rho_{mn}^{\mathbf{q}}(\mathbf{r}) \approx c_\alpha^{\mathbf{q}}\chi_\alpha^{\mathbf{q}}(\mathbf{r})$, into the desired four centre integral yields,

$$\int \mathrm{d}\mathbf{r}\,\mathrm{d}\mathbf{r}' \frac{\rho_{mn}^{\mathbf{q}}(\mathbf{r})\rho_{rs}^{\mathbf{q}*}(\mathbf{r}')}{|\mathbf{r}-\mathbf{r}'|} \approx c_\alpha^{\mathbf{q}} \int \mathrm{d}\mathbf{r}\,\mathrm{d}\mathbf{r}' \frac{\chi_\alpha^{\mathbf{q}}(\mathbf{r})\rho_{rs}^{*\mathbf{q}}(\mathbf{r}')}{|\mathbf{r}-\mathbf{r}'|}. \tag{12}$$

Together with the expansion coefficients from Equation (9),

$$c_\alpha^{\mathbf{q}} = V_{mn\beta}^{\mathbf{q}} V_{\beta\alpha}^{\mathbf{q}-1}, \tag{13}$$

this yields,

$$\int \mathrm{d}\mathbf{r}\,\mathrm{d}\mathbf{r}' \frac{\rho_{mn}^{\mathbf{q}}(\mathbf{r})\rho_{rs}^{\mathbf{q}*}(\mathbf{r}')}{|\mathbf{r}-\mathbf{r}'|} \approx V_{mn\beta}^{\mathbf{q}} V_{\beta\alpha}^{\mathbf{q}-1} V_{\beta rs}^{\mathbf{q}*}, \tag{14}$$

where $V_{\alpha\beta}^{\mathbf{q}-1}$ is the matrix inverse of $V_{\alpha\beta}^{\mathbf{q}}$. The integrals in Equations (10) and (11) are lattice modulated Ewald sums and are evaluated using standard Ewald methods [39].

3. Results

In this section, TDHF and BSE calculations for free molecules, with and without the TDA approximation, are compared to previous CASPT2 [7], CMRCI-Q [9] and EOM-CCSD [10] calculations. The latter all used extensive diffuse basis sets capable of capturing several principal quantum numbers of Rydberg states. The TZVPPD basis sets used in this work contain a more limited set of diffuse functions, yet energies of low-lying states from TDHF and BSE agree well with the more expensive methods listed. For small molecules such as C_2H_2, level shifts due to screening in *GW* and BSE calculations are small and BSE and TDHF calculations of dipole susceptibilities generally agree well [24].

At present, only TDHF-TDA calculations on periodic systems are possible within the Exciton code [39], while TDHF and BSE calculations (using both *A* and *B* matrices in Equation (1)) are possible within the molecular version of the code [24]. As noted above, diffuse GTO basis functions cause numerical problems in periodic SCF calculations. Hence a modified basis with the most diffuse basis functions removed[1] was used in calculations on the C_2H_2 molecular crystal. Results of TDHF-TDA molecule-in-a-box calculations, with a single C_2H_2 molecule in a $15 \times 15 \times 15 Å^3$ unit cell repeated periodically in space, are compared to free molecule calculations using the full TZVPPD basis sets for C and H and the modified TZVPPD basis sets used for the molecular crystal, to determine the effect of the reduced basis on molecular excitation energies. The box in these calculations is large enough to avoid numerical problems associated with diffuse functions when it contains only one molecule. The molecular crystal environment is different, of course, since molecules are much more densely packed and the space around a molecule is partly expanded by basis functions on neighbouring molecules. Thus far GTO basis sets for periodic calculations are mainly determined using a variational approach in which the most diffuse GTO exponents are adjusted to minimise the total energy in SCF calculations, while rejecting exponents below 0.1 a_o^{-2} [40]. A more systematic approach to selecting basis sets optimised for excited state calculations is desirable.

3.1. Molecular excitations

Low-lying excitations of C_2H_2 are comprised of transitions from the π_u HOMO level. Singlet excited states which arise from direct products of these orbitals with virtual states of various symmetries and their optical activities are given in Table 2.

Single-particle energy levels for HF and *GW* calculations on single molecules and for HF calculations in a cubic unit cell of side 15 Å(molecule-in-box), repeated periodically are given in Table 3. Occupied state HF levels are shifted upwards by 0.06 –0.10 eV on going from the TZVPPD basis to the modified basis or from free molecule to periodic calculation. Virtual state levels are affected to a larger extent, for example, the $4\sigma_g$ level is shifted upwards by 0.69 eV on going from the free molecule to the molecule with periodic boundary conditions and by 2.27 eV in the free molecule on going from the TZVPPD basis to the modified basis (Table 3).

GW quasiparticle corrections to HF single-particle levels in the free molecule are small. Occupied σ levels are shifted upwards, while there is a small downwards shift of the π_u level. There is therefore excellent agreement between the experimental ionisation potential (11.40 eV [18]) and this level for both HF and *GW* (11.32 and 11.37 eV, respectively). An electron scattering study on C_2H_2 found a π^* resonance at 2.6 eV [41], which compares to $1\pi_g$ virtual state HF and *GW* levels at 3.99 and 3.54 eV.

Vertical excitation energies for TDHF and BSE calculations for the free C_2H_2 molecule, with and without the TDA, are compared to CASPT2, CMRCI+Q and EOM-CCSD calculations in Table 4. The HF equilibrium geometry for the TZVPPD basis is $r_{CC} = 1.180$ Åand $r_{CH} = 1.055$ Å. This compares to $r_{CC} = 1.210$ Å, r_{CH}

Table 2. Direct products of the π_u HOMO levels in C_2H_2 with low-lying virtual levels under D_{2h} point symmetry and their associated excited state term symbols and dipole activity.

Transition	Singlet excited states	Dipole activity
$\pi_u \otimes \sigma_g^*$	$^1\Pi_u$	(x, y)
$\pi_u \otimes \sigma_u^*$	$^1\Pi_g$	0
$\pi_u \otimes \pi_g^*$	$^1\Sigma_u^+ \oplus {}^1\Sigma_u^- \oplus {}^1\Delta_u$	z, 0, 0
$\pi_u \otimes \pi_u^*$	$^1\Sigma_g^- \oplus {}^1\Sigma_g^+ \oplus {}^1\Delta_g$	0, 0, 0
$\pi_u \otimes \delta_g^*$	$^1\Phi_u$	0

Table 3. Single-particle energy levels in eV from HF and *GW* calculations on C_2H_2.

Level	HF[a,c]	HF[b,c]	*GW*[b,c]	HF[a,d]	HF[b,d]
$2\sigma_u$	−20.79	−20.85	−19.69	−20.73	−20.79
$3\sigma_g$	−18.55	−18.61	−17.58	−18.49	−18.55
$1\pi_u$	−11.26	−11.32	−11.37	−11.16	−11.22
$4\sigma_g$	2.69	2.00	1.82	5.90	4.27
$3\sigma_u$	3.60	2.47	2.26	6.13	4.63
$1\pi_g$	4.26	3.99	3.54	5.25	5.18
$5\sigma_g$	5.22	4.18	3.94	9.14	8.23
$4\sigma_u$	8.75	5.82	5.58	12.47	11.10

Notes: Data presented in the first three columns are for single molecules in free space. Data presented in the last two columns are for periodic arrays of single molecules in $15 \times 15 \times 15$ Å^3 unit cells. HF single-particle levels are compared using a full TZVPPD basis or the modified TZVPPD basis used for calculations on the C_2H_2 molecular crystal.
[a] Molecule in box.
[b] Single molecule.
[c] TZVPPD.
[d] Mod. TZVPPD.

Table 4. Vertical excitation energies from the C_2H_2 ground state in eV.

Term	Orbital	TDHF	TDHF-TDA	BSE	BSE-TDA	CASPT2[a]	CMRCI+Q[b]	EOM-CCSD[c]
$1^1\Sigma_u^-$	π_g	6.35	6.68	6.65	6.94	7.07	–	7.12
$1^1\Delta_u$	π_g	6.86	7.02	7.13	7.27	7.40	–	7.44
$1^1\Pi_u$	σ_g	8.51	8.52	8.45	8.47	8.30	8.25	8.31
$1^1\Pi_g$	σ_u	9.16	9.16	9.05	9.06	8.60	8.67	8.70
$2^1\Pi_u$	σ_g	10.14	10.17	10.09	10.11	9.55	9.52	9.53
$1^1\Sigma_u^+$	π_g	10.59	11.07	10.39	10.77	9.65	9.65	9.69
$1^1\Delta_g$	π_u	11.64	11.65	11.53	11.54	8.96	9.08	9.15
$1^1\Sigma_g^-$	π_u	11.64	11.67	11.53	11.56	8.92	9.16	
$2^1\Pi_g$	σ_u	12.04	12.07	11.94	11.96		10.17	
$1^1\Phi_u$	δ_g	12.52	12.53	12.49	12.50	9.93	9.97	
$1^1\Sigma_g^+$	π_u	12.69	12.80	12.47	12.57	9.06	9.24	9.36

Notes: TDHF and BSE calculations in this work were performed at the ground state HF equilibrium geometry using TZVPPD basis sets. The column labelled orbital gives the character of the excited orbital in each excited state.
[a] Ref.[7].
[b] Ref.[9].
[c] Ref.[10].

$= 1.065$ Åin a CMRCI+Q with a VTZ+Ryd basis [9], $r_{CC} = 1.211$ Å, $r_{CH} = 1.061$ Åin a HF+MP2 calculation with a ccp-VTZ basis [10], $r_{CC} = 1.217$ Å, $r_{CH} = 1.066$ Åin a CASPT2 calculation [7] and $r_{CC} = 1.203$ Å, $r_{CH} = 1.062$ Åin experiment [42].

The $1^1\Sigma_u^-$ lowest vertical excitation energy is predicted to lie between 6.3 and 6.9 eV by TDHF and BSE methods and at 7.1 eV by CASPT2 and EOM-CCSD (Table 4). For most excited states listed in Table 4, the TDA makes only a small difference to BSE or TDHF energies. Notable exceptions are the $^1\Sigma_u^-$ and $^1\Sigma_u^+$ states, where removing the TDA results in a lowering of the TDHF-TDA excited state energy by 0.33 and 0.48 eV, respectively, and by similar amounts on removing the TDA in BSE-TDA calculations. In both cases, the orbitals to which the excited electron is transferred are π_g orbitals. The TDA has much less effect when excitation is to σ_u or σ_g orbitals in the $^1\Pi_u$ or $^1\Pi_g$ states. TDHF and BSE energies for the $1^1\Delta_u$ state are up to 0.5 eV below the predicted CASPT2 and EOM-CCSD energies. For higher excited states the TDHF and BSE excitation energies are higher than the more accurate CI and CCSD methods. However, in the C_2H_2 molecular crystal the focus will be on these low energy excitations.

3.2. Molecular versus molecule-in-box excitations

In order to draw comparisons between calculations on the free molecule and in the condensed phase, calculations were performed on single C_2H_2 molecules in large, cubic unit cells with lattice constant 15 Å. It should be noted that Coulomb and exchange integrals in TDHF or BSE methods in Exciton [24,39] are computed in entirely different ways in free molecule versus periodic calculations. In the former, the Coulomb interaction is in real space and in the latter it is handled as an Ewald potential. TDHF-TDA excitation energies for C_2H_2 as free molecules or in large unit cells are compared in Table 5 in full TZVPPD and modified TZVPPD bases. Molecule-in-box excitation energies in Table 5 have been extrapolated to infinite $\mathbf{q}$ sampling density. The lowest two excitation energies agree remarkably well. In the full TZVPPD basis they agree to within 0.01 eV and in the modified basis they agree to within 0.1 eV. Excitations below 12 eV for the full TZVPPD basis for the free molecule and the molecule-in-box calculations differ by up to 0.3 eV and by more for the modified TZVPPD basis. The lowest excitations are localised, molecular excitations with zero dipole activity. Good agreement between the two methods can therefore be expected in this case. Higher excitations are to Rydberg like states. The basis of crystal orbitals available for excitations of the molecule-in-box is quite different from the entirely localised basis available for excitations of the free molecule in that case and differences in excitation energies can be expected.

Table 5. TDHF-TDA excitation energies in eV from single molecule and molecule-in-box calculations using the TZVPPD and modified TZVPPD bases.

Term	Mol.[a]	Mol-in-box[a]	Mol.[b]	Mol-in-box[b]
$1^1\Sigma_u^-$	6.68	6.67	6.75	6.85
$1^1\Delta_u$	7.02	7.02	7.12	7.21
$1^1\Pi_u$	8.52	8.77	9.89	10.64
$1^1\Pi_g$	9.16	9.70	10.25	11.05
$2^1\Pi_u$	10.17	10.47	11.81	12.35
$1^1\Sigma_u^+$	11.07	11.31	12.44	12.51
$1^1\Delta_g$	11.65	11.95	14.31	14.46
$1^1\Sigma_g^-$	11.66	11.96	14.41	15.42
$2^1\Pi_g$	12.06	12.54	14.38	14.67

[a] TZVPPD basis.
[b] modified TZVPPD basis (see endnote 1).

Optical absorption spectra from TDHF-TDA calculations are shown in Figure 1 for the optical field parallel or perpendicular to the molecular axis. The single molecule TZVPPD spectrum shown in Figure 1(e) corresponds to excitation energies in the second column of Table 4.

Figure 1(c) shows the calculation on a molecule with the same basis but repeated periodically. The main features of the optical response are similar in either case. Optical cross sections for free/periodically repeated molecules were calculated using the length/velocity gauges. No correction was made for interaction between the molecular transition dipoles in the molecule-in-box calculations. There is an upward shift in excitation energies when the modified TZVPPD basis is used (Figure 1(b,d)).

3.3. Condensed phase excitations

The HF band structure of C_2H_2 in the cubic phase using atomic coordinates from experiment [14] is shown in Figure 2. The figure shows the first complex of 16 conduction band states, comprised of four $4\sigma_g$, four $3\sigma_u$ and eight $1\pi_g$ molecular virtual states. It also shows the eight bands formed from molecular $1\pi_u$ occupied states and all bands ranging from $2\sigma_g$ up to 40 eV. In the molecular crystal HF calculation at the Γ point of the Brillouin zone, the $4\sigma_g$ and $3\sigma_u$ levels shift upwards by 2.2 eV, the $1\pi_g$ level shifts upwards by 1.1 eV and the $5\sigma_g$ and $4\sigma_u$ levels shift upwards by several eV, relative to the free molecule. The TDHF-TDA calculations reported here used the $2\sigma_u$, $3\pi_g$, $1\pi_u$ bands and all virtual bands up to 30 eV in the active space.

The T_h crystallographic point group of the $Pa\bar{3}$ space group to which the cubic phase of C_2H_2 belongs, has A_g, E_g, T_g, A_u, E_u and T_u representations. The 14 lowest excitation energies for the cubic phase of C_2H_2 are shown in Table 6, together with their degeneracy (as T-triply, E-doubly or A-singly degenerate) and their optical activity. The excited states are grouped as 12 low energy states (including degeneracy factors) around 7.3 and 7.8 eV and they split into 4 and 8 states at these energies. Only the triply degenerate state at 7.77 is (weakly) optically active in this energy range. This appears as a small feature in the optical absorption spectrum in Figure 1(a). The next optically active excitation is the strongest optical absorption predicted in the VUV energy range at 10.15 eV and there is a weaker absorption at 10.40 eV.

Eigenvectors in TDHF-TDA or BSE-TDA calculations (Equation (1)) are linear combinations of electron-hole pair probability amplitudes,

$$\Psi(1,2) = \sum_{i,a} X_{ia}\phi_i(1)\phi_a^*(2), \qquad (15)$$

where X_{ia} is an eigenvector component, $\phi_i(1)$ and $\phi_a(2)$ are hole and electron wave functions, either Bloch functions or molecular orbitals. Plots of electron probability density for a fixed hole position reveal electron-hole

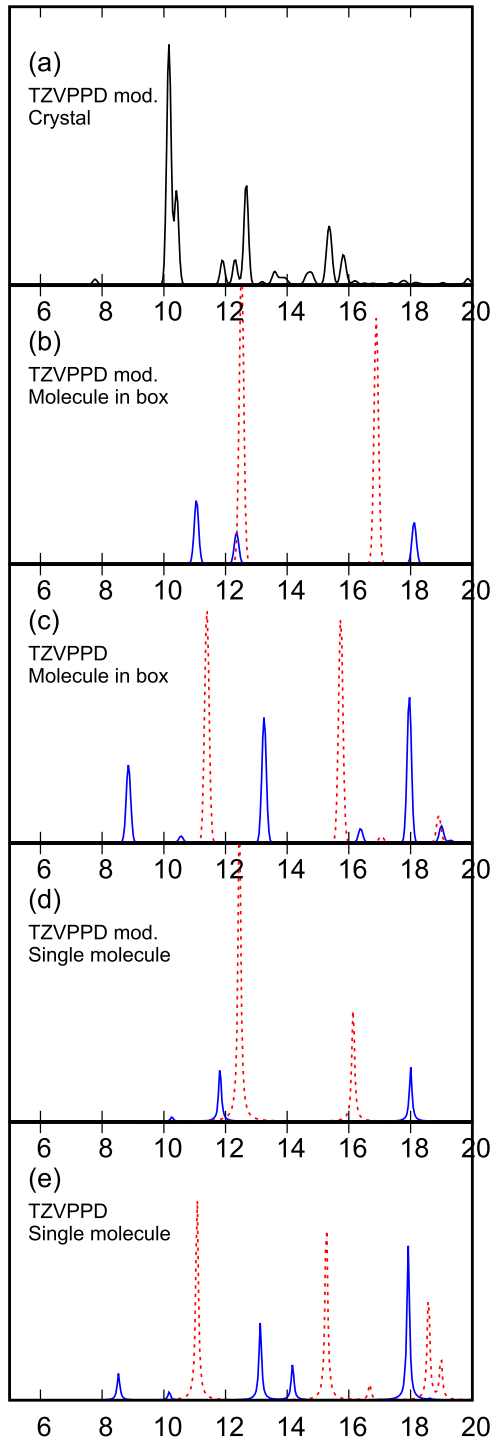

Figure 1. (Color online) Predicted optical absorption spectra for molecular and crystalline C_2H_2. (a) Molecular crystal, (b), (c) single molecule in unit cell $15 \times 15 \times 15$ Å^3 with TZVPPD or modified TZVPPD basis, (d), (e) single molecule in free space with TZVPPD or modified TZVPPD basis. Solid blue and dotted red lines in (b) to (e) indicate a transition dipole moment perpendicular or parallel to the molecular axis, respectively. The intensity of the molecular crystal absorption relative to the periodically repeated molecule calculations has been adjusted for molecular density and orientation.

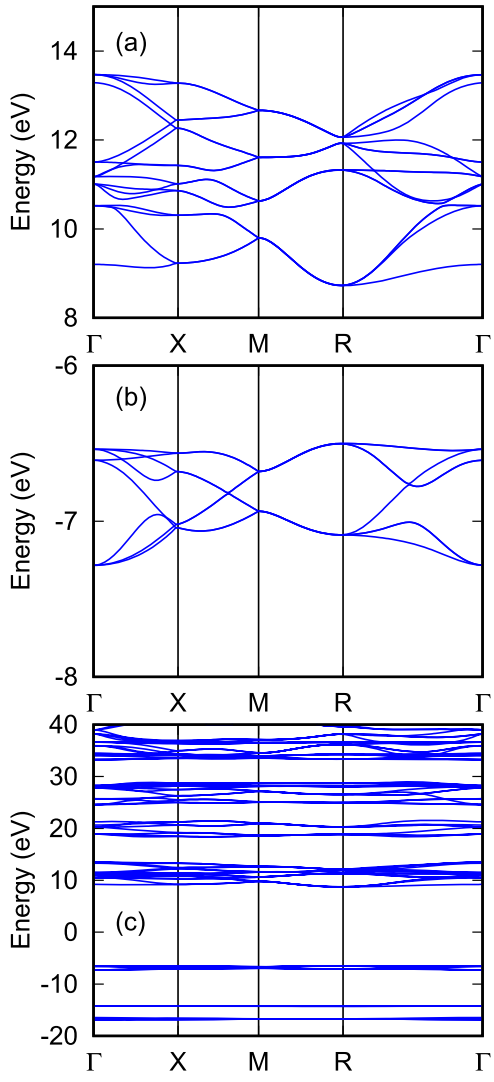

Figure 2. (Color online) Band structure of C_2H_2. (a) Complex of first 16 virtual states with $4\sigma_g$, $1\pi_g$ and $5\sigma_u$ character. (b) 8 $1\pi_u$ valence band states. (c) Valence band and virtual states ranging from $2\sigma_g$ up to 40 eV.

Table 6. TDHF-TDA low energy excitation energies of the C_2H_2 molecular crystal in eV.

Degeneracy	Energy	Optical activity
T	7.31	N
A	7.32	N
E	7.75	N
T	7.76	N
T	7.77	Y
T	10.15	Y
E	10.21	N
T	10.40	Y
T	10.81	N
E	10.81	N
T	10.82	N
T	11.88	N
T	11.91	Y
E	11.96	N

Note: The degeneracy and optical activity of each state are also shown.

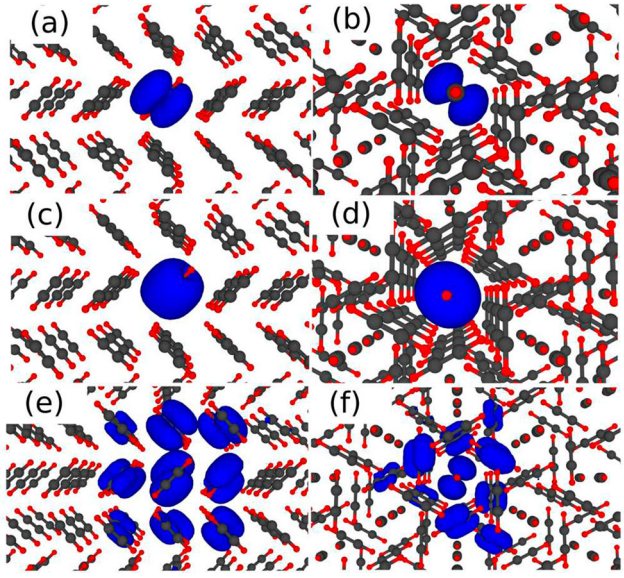

Figure 3. (Color online) Electron distributions in correlated electron-hole pairs with holes located just off the molecular axis in the central molecule. (a), (b) Localised state at 7.31 eV. (c), (d) Localised state at 7.75 eV. (e), (f) Partly delocalised state at 12.26 eV. Left panels: view along (001) axis, right panels: view along (111) axis.

correlations in excited states. The excited states in C_2H_2 investigated here all involve π_u hole states which have nodal planes along the molecular axis. In order to visualise the electron probability density for C_2H_2, the fixed hole position must therefore lie off the molecular axis. Electron probability density plots for a hole fixed just off the molecular axis and near the C atoms in the molecule are shown for three excited states in Figure 3. The states selected are the lowest excited state at 7.31 eV and states at 7.75 and 12.26 eV. The first two are localised states in which the electron and hole are confined to the same molecule and the latter shows partial delocalisation of the electron.

The plot for the state at 7.31 eV in Figure 3(a,b) shows a π-like electron distribution about the bond axis. It is entirely localised on that molecule and can be interpreted as a state derived from the molecular $1^1\Sigma_u^-$ state, where it had energy 6.85 eV in the same basis in the molecule-in-box calculation (Table 5). The plot for the state at 7.75 eV in Figure 3(c,d) shows a σ-like electron distribution about the bond axis. These results and the number of states at each energy are consistent with linear combinations of $^1\Delta_u$ states for the group of states at 7.8 eV. Note that neither the $1^1\Sigma_u^-$ nor $1^1\Delta_u$ states is dipole active in the free molecule and that there is a weak optical acitivity of the excitation at 7.77 eV.

Orbital angular momentum about the molecular axis in axially symmetric molecules is quantised in units of $\hbar$, with quantum number Λ. Eigenfunctions of

$\hat{L}_z = \hat{l}_z(1) + \hat{l}_z(2)$, where z is the molecular axis, which are symmetric with respect to space coordinates and have spin singlet total wave functions, have the forms,

$$\Psi(1,2)_{\Lambda=0} = \frac{1}{\sqrt{2}}(\pi_{ux}(1)\pi_{gx}(2) + \pi_{uy}(1)\pi_{gy}(2)), \tag{16}$$

$$\Psi(1,2)_{\Lambda=-2} = \frac{1}{2}\big[(\pi_{ux}(1)\pi_{gx}(2) - \pi_{uy}(1)\pi_{gy}(2)) - i(\pi_{ux}(1)\pi_{gy}(2) + \pi_{uy}(1)\pi_{gx}(2))\big], \tag{17}$$

and

$$\Psi(1,2)_{\Lambda=+2} = \frac{1}{2}\big[(\pi_{ux}(1)\pi_{gx}(2) - \pi_{uy}(1)\pi_{gy}(2)) + i(\pi_{ux}(1)\pi_{gy}(2) + \pi_{uy}(1)\pi_{gx}(2))\big]. \tag{18}$$

Here u, g and x, y refer to ungerade and gerade π_x and π_y orbitals which are occupied and unoccupied in the ground state. Coordinates (1) and (2) refer to hole and particle coordinates in the excited state. In the free molecular case, where wavefunctions are restricted to being real, the configurations which appear in the $|\Lambda| = 2$, $^1\Delta_u$ state are the linear combinations $\frac{1}{\sqrt{2}}(\pi_{ux}(1)\pi_{gx}(2) - \pi_{uy}(1)\pi_{gy}(2))$ and $\frac{1}{\sqrt{2}}(\pi_{ux}(1)\pi_{gy}(2) + \pi_{uy}(1)\pi_{gx}(2))$. Fixing the hole position so that, for example, $\pi_{ux}(1) = 0, \pi_{uy}(1) \neq 0$ in Equation (16) results in a particle probability density which is $|\pi_{gy}(2)|^2$ and a π-like probability distribution is expected for localised states derived from the $^1\Sigma_u^-$ molecular state (Figure 3(a,b)). Similarly, fixing the hole position so that $\pi_{ux}(1) = 0, \pi_{uy}(1) \neq 0$ in Equation (16) or (17) results in a particle probability distribution which is $|\pi_{gx}(2) \pm i\pi_{gy}(2)|^2$ and a cylindrically symmetric particle probability density is expected for localised states derived from the $^1\Delta_u$ molecular state (Figure 3(c,d)). Since these are localised, essentially molecular excited states, it is likely that their equilibrium geometries are bent, as in the free molecule [19].

A further group of six states exists between 10.15 and 10.82 eV. Among these, the triply degenerate states at 10.15 and 10.40 eV are optically active. The next two excitations in the spectrum of excited states of the free molecule are the $1^1\Pi_u$ and $1^1\Pi_g$ states. These states are found at 10.64 and 11.05 eV (in the free molecule using the modified TZVPPD basis). States of $^1\Pi_u$ symmetry are optically active in the free molecule. Unlike the excitations around 7.3 and 7.8 eV, where the electron and hole are localised on the same molecule, in this case and for higher energy excitations, the electron and hole may separate by up to one or two shells of neighbouring molecules. A plot of a non-degenerate electron distribution in an excited state at 12.26 eV is shown in Figure 3(e,f).

The character of low-lying excitations in organic molecular crystals has been investigated previously using BSE methods, especially polyacenes where there is the possibility of hybrid internal Frenkel excitons and charge transfer states [43–45]. In contrast, excitations in C_2H_2 are either entirely localised, in which case the carbon triple bond is disrupted and the excited state equilibrium geometry is bent with a carbon-carbon bond length typical of a carbon double bond, suggesting an open-shell singlet diradical character for the excited state. The free molecule HF IP of C_2H_2 in the modified TZVPPD basis is 11.22 eV (Table 3). The distance between nearest neighbour molecular centres is 4.3 Å. The Coulombic stabilisation of an electron and hole separated by this distance is around 3.3 eV. Excited states with energies greater than 11.2–3.3 = 7.9 eV can therefore be expected to be at least partly delocalised and are therefore of predominantly charge transfer character.

4. Summary

TDHF and BSE calculations, with and without the Tamm–Dancoff approximation, have been performed for C_2H_2 and compared to CASPT2, CMRCI+Q and EOM-CCSD calculations in the literature. Characters of excited states were determined by inspecting excited state configurations in TDHF or BSE eigenvectors. Resulting excitation energies are in reasonably good agreement with the more accurate and expensive calculations noted. Results of calculations for single molecules in free space and molecule-in-box periodically repeated arrays are compared for the TZVPPD and modified TZVPPD basis sets used in this work. Finally, TDHF-TDA calculations are performed for the C_2H_2 molecular crystal and low energy excitations are analysed and compared to those of the free molecule. Plots of correlated electron-hole probability density show that the two lowest excitations in the condensed phase resemble the two lowest $^1\Sigma_u^-$ and $^1\Delta_u$ 'valence' excitations of the free molecule.

Note

1. The TZVPPD C basis was modified by replacing the two most diffuse *s* exponents by one exponent of 0.129, increasing the most diffuse *p* exponent from 0.100 to 0.129 and removing the most diffuse *d* and *f* exponents. The TZVPPD H basis was modified by removing the most diffuse *p* exponent.

Acknowledgements

This work was supported by TCHPC (Research IT, Trinity College Dublin). Calculations were performed on the Boyle and

Kelvin clusters maintained by the Trinity Centre for High Performance Computing. The Boyle cluster was funded through grants from the European Research Council and Science Foundation Ireland. The Kelvin cluster was funded through grants from the Irish Higher Education Authority, through its PRTLI programme.

Disclosure statement

No potential conflict of interest was reported by the author.

References

[1] T.M. Burke, S. Sweetnam, K. Vandewal and M.D. McGehee, Adv. Energy Mater. **5**, 1500123 (2015).
[2] M. Azzouzi, T. Kirchartz and J. Nelson, Trends Chem. **1**, 49 (2019).
[3] G. Cooper, G.R. Burton and C.E. Brion, J. Electron. Spectrosc. Relat. Phenom. **73**, 139 (1995).
[4] M. Kono, K. Hoshina and K. Yamanouchi, J. Chem. Phys. **117**, 1040 (2002).
[5] B.-M. Cheng, H.-F. Chen, H.-C. Lu, H.-K. Chen, M.S. Alam, S.-L. Chou and M.-Y. Lin, Astrophys. J. Suppl. Ser. **196**, 3 (2011).
[6] Y.-W. Liu, L.-Q. Xu, T. Chen, D.-G. Qi, T. Xiong and L.-F. Zhu, Astrophys. J. Suppl. Ser. **234**, 10 (2018).
[7] K. Malsch, R. Rebentisch, P. Swiderek and G. Hohlneicher, Theor. Chem. Acc. **100**, 171 (1998).
[8] A.S. Zyubin and A.M. Mebel, J. Chem. Phys. **119**, 6581 (2003).
[9] F. Laruelle, S. Boyé-Péronne, D. Gauyacq and J. Liévin, J. Phys. Chem. A **113**, 13210 (2009).
[10] N. Watanabe and M. Takahashi, J. Phys. B. At. Mol. Opt. Phys. **53**, 075202 (2020).
[11] L. Hedin, Phys. Rev. **139**, A796 (1965).
[12] W. Hanke and L.J. Sham, Phys. Rev. Lett. **43**, 387 (1979).
[13] G. Strinati, R. Nuovo Cimento **11**, 1 (1988).
[14] R.K. McMullan, A. Kvick and P. Popelier, Acta Cryst. B **48**, 726 (1992).
[15] F. Bruneval, S.M. Hamed and J.B. Neaton, J. Chem. Phys. **142**, 244101 (2015).
[16] D. Jacquemin, I. Duchemin and X. Blase, J. Chem. Theory Comput. **11**, 3290 (2015).
[17] X. Gui, C. Holzer and W. Klopper, J. Chem. Theory Comput. **14**, 2127 (2018).
[18] P. Rupper and F. Merkt, Rev. Sci. Instrum. **75**, 613 (2004).
[19] S.P. So, R.W. Wetmore and H.F. Schaefer III, J. Chem. Phys. **73**, 5706 (1980).
[20] F. Weigend and R. Ahlrichs, Phys. Chem. Chem. Phys. **7**, 3297 (2005).
[21] D. Rappoport and F. Furche, J. Chem. Phys. **133**, 134105 (2010).
[22] B.P. Pritchard, D. Altarawy, B. Didier, T.D. Gibsom and T.L. Windus, J. Chem. Inf. Model. **59**, 4814 (2019).
[23] C.H. Patterson, Mol. Phy. **108**, 3181 (2010).
[24] C.H. Patterson, Phys. Rev. Mater. **3**, 043804 (2019).
[25] W.C. Price, Phys. Rev. **47**, 444 (1935).
[26] M. Perić, R.J. Buenker and S.D. Peyerimhoff, Mol. Phys. **53**, 1177 (1984).
[27] M. Perić, S.D. Peyerimhoff and R.J. Buenker, Mol. Phys. **62**, 1339 (1987).
[28] M. Perić and S.D. Peyerimhoff, in *Understanding Chemical Reactivity – The Role of Rydberg States in Spectroscopy and Photochemistry. Low and High Rydberg States*, edited by C. Sandorfy (Kluwer Academic Publishers, Dordrecht, NL, 1999), pp 137–178.
[29] J.L. Whitten, J. Chem. Phys. **58**, 4496 (1973).
[30] B.I. Dunlap, J.W.D. Connolly and J.R. Sabin, J. Chem. Phys. **71**, 3396 (1979).
[31] B.I. Dunlap, J. Mol. Struct. Theochem. **501**, 221 (2000).
[32] J.W. Mintmire, J.R. Sabin and S.B. Trickey, Phys. Rev. B **26**, 1743 (1982).
[33] L. Maschio, D. Usvyat, F.R. Manby, S. Casassa, C. Pisani and M. Schütz, Phys. Rev. B **76**, 075101 (2007).
[34] M. Milko, J. Noga and S. Varga, Int. J. Quant. Chem. **107**, 2158 (2007).
[35] A.M. Burow, M. Sierka and F. Mohamed, J. Chem. Phys. **131**, 214101 (2009).
[36] B.I. Dunlap, N. Rösch and S.B. Trickey, Mol. Phy. **108**, 3167 (2010).
[37] M. Lorenz, L. Maschio, M. Schütz and D. Usvyat, J. Chem. Phys. **137**, 204119 (2012).
[38] Q. Sun, T.C. Berkelbach, J.D. McClain and G.K.-L. Chan, J. Chem. Phys. **147**, 164119 (2017).
[39] C.H. Patterson, arXiv:2005.09291.
[40] R. Dovesi, A. Erba, R. Orlando, C.M. Zicovich-Wilson, B. Civalleri, L. Maschio, M. Rerat, S. Casassa, J. Baima, S. Salustro and B. Kirtman, WIREs Comput. Mol Sci. **8**, e1360 (2018).
[41] R. Dressler and M. Allan, J. Chem. Phys. **87**, 4510 (1987).
[42] A. Baldacci, S. Ghersetti, S.C. Hurlock and K.N. Rao, J. Mol. Spectrosc. **59**, 116 (1976).
[43] K. Hummer, P. Puschnig and C. Ambrosch-Draxl, Phys. Rev. Lett. **92**, 147402 (2004).
[44] B. Baumeier, D. Andrienko and M. Rohlfing, J. Chem. Theory Comput. **8**, 2790 (2012).
[45] P. Cudazzo, M. Gatti, A. Rubio and F. Sottile, Phys. Rev. B **88**, 195152 (2013).